Lab on a Chip

Miniaturisation for chemistry, physics, biology, materials science and bioengineering

www.rsc.org/loc

Volume 12 | Number 10 | 24 April 2012 | Pages 1725–1904

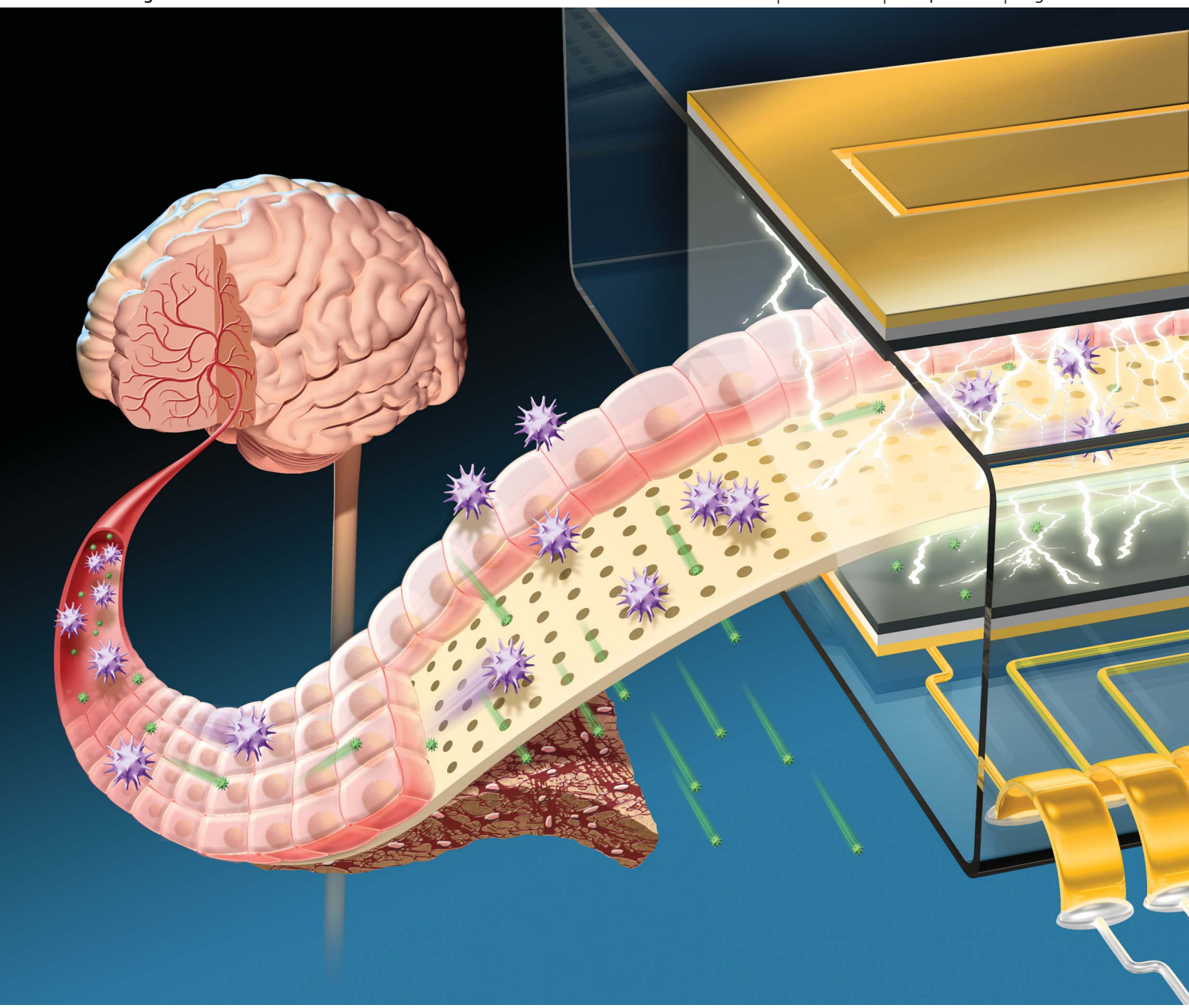

ISSN 1473-0197

RSC Publishing

PAPER

Ross Booth and Hanseup Kim

Characterization of a microfluidic *in vitro* model of the blood-brain barrier (μBBB)

Lab on a Chip

Dynamic Article Links

Cite this: *Lab Chip*, 2012, **12**, 1784

www.rsc.org/loc

PAPER

Characterization of a microfluidic *in vitro* model of the blood-brain barrier (μBBB)

Ross Booth[*a] **and Hanseup Kim**[*b]

Received 24th January 2012, Accepted 29th February 2012
DOI: 10.1039/c2lc40094d

The blood-brain barrier (BBB), a unique selective barrier for the central nervous system (CNS), hinders the passage of most compounds to the CNS, complicating drug development. Innovative *in vitro* models of the BBB can provide useful insights into its role in CNS disease progression and drug delivery. Static transwell models lack fluidic shear stress, while the conventional dynamic *in vitro* BBB lacks a thin dual cell layer interface. To address both limitations, we developed a microfluidic blood-brain barrier (μBBB) which closely mimics the *in vivo* BBB with a dynamic environment and a comparatively thin culture membrane (10 μm). To test validity of the fabricated BBB model, μBBBs were cultured with b.End3 endothelial cells, both with and without co-cultured C8-D1A astrocytes, and their key properties were tested with optical imaging, *trans*-endothelial electrical resistance (TEER), and permeability assays. The resultant imaging of ZO-1 revealed clearly expressed tight junctions in b. End3 cells, Live/Dead assays indicated high cell viability, and astrocytic morphology of C8-D1A cells were confirmed by ESEM and GFAP immunostains. By day 3 of endothelial culture, TEER levels typically exceeded 250 Ω cm^2 in μBBB co-cultures, and 25 Ω cm^2 for transwell co-cultures. Instantaneous transient drop in TEER in response to histamine exposure was observed in real-time, followed by recovery, implying stability of the fabricated μBBB model. Resultant permeability coefficients were comparable to previous BBB models, and were significantly increased at higher pH (>10). These results demonstrate that the developed μBBB system is a valid model for some studies of BBB function and drug delivery.

Introduction

Diseases of the central nervous system (CNS) present a prevalent and ever increasing burden for the world healthcare industry. For example, Alzheimer's disease is diagnosed in an estimated 24 million people, a number projected to double every 20 years.[20] Despite such emerging demands for treatment of CNS diseases, only 7% of CNS drugs in clinical development reach the marketplace (Fig. 1A), compared to the 12% average across all therapeutic areas, or 20% for cardiovascular drugs.[19,21]

This low success rate is attributed primarily to a unique CNS structure coined as the blood-brain barrier (BBB),[21] which introduces a pharmacokinetic hurdle by blocking compounds from entering brain tissues from capillaries.[22] Only compounds smaller than about 500 Da easily cross the BBB, but few CNS diseases consistently respond to this category of molecules.[23]

Because the BBB blocks nearly all polar or large compounds, new drug treatments for the CNS of higher molecular weight must take BBB function into account, requiring more extensive pre-clinical studies. The use of *in vitro* models of the BBB would augment the conventional pharmaceutical approach focusing on drug design, help predict the penetration of drug candidates across the BBB,[24] and allow pre-screening and optimization of new treatments prior to animal and clinical studies.[25] BBB models can also be used to study the role of barrier function on CNS disease progression,[26] and test innovative methods of delivery.[27]

BBB studies have been performed largely in two platforms: *in vivo* and *in vitro* models (Tab. 1). *In vivo* models directly utilize entire living organisms, typically rats or mice, while *in vitro* models construct artificial environments with cultured cells to mimic *in vivo* structures. *In vitro* models are a valuable pre-cursor to animal models due to lower cost, time, and ethical constraints. More specific to the BBB, unlike in animal studies, *in vitro* models enable controlled, repeatable, and non-invasive tests: permeability assays, resistance measurements, and microscopy.

Although traditional *in vivo* models provide environments closer to the human phenotype, they cannot provide massively-parallel, controlled, and repeatedly identical environments for reliable and quantitative studies (Table 1). More importantly in terms of practicality, *in vivo* models require extraordinary

[a]*Department of Bioengineering, University of Utah, MEB-1445, 50 S Central Campus Dr, Salt Lake City, UT, USA 84112. E-mail: Ross.Booth@utah.edu; Tel: +1 801 587 3351*
[b]*Department of Electrical & Computer Engineering, University of Utah, MEB-2278, 50 S Central Campus Dr, Salt Lake City, UT, USA 84112. E-mail: hanseup.kim@utah.edu; Tel: +1 801 587 9497*

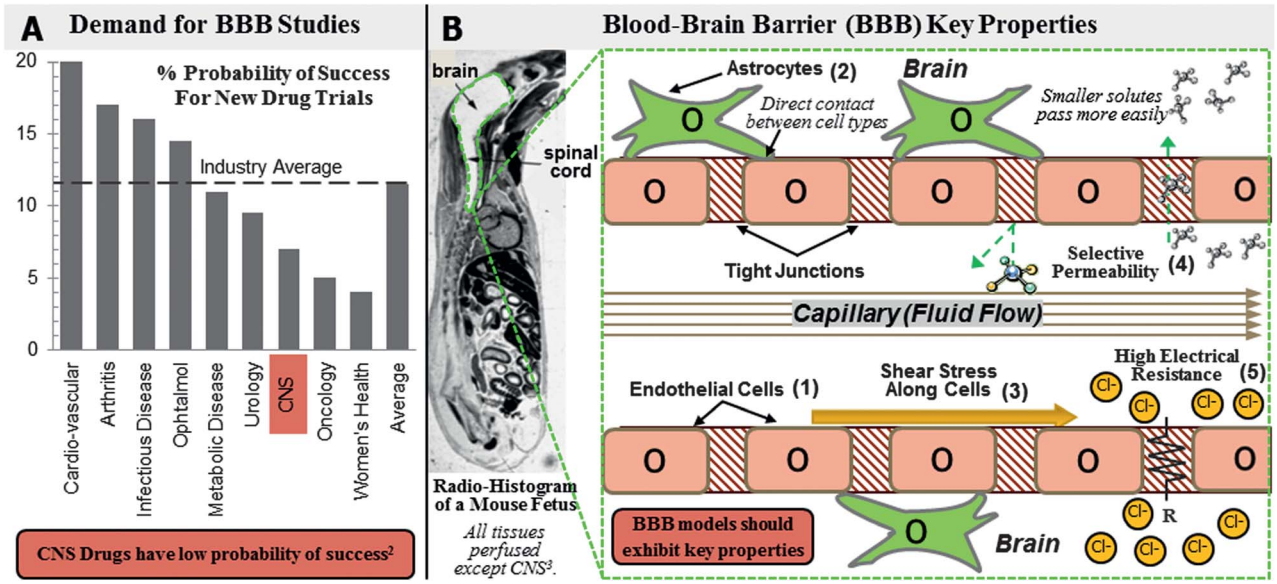

Fig. 1 Motivation and background for μBBB development. (A) Probability of success is lower for new CNS drugs than those in other healthcare areas due to the unique architecture of brain capillaries.[19] (B) The CNS is unique due to the extraordinary selectivity of the BBB.[21] Better model systems of the BBB will contribute to development of CNS disease treatments. Effective *in vitro* BBB models should successfully include key properties: (1) endothelial cells with tight junction expression; (2) co-culture with astrocytes; (3) presence of shear stress; (4) selective permeability to compounds; (5) high electrical resistance across tight junctions.

amounts of cost, time, and man-hours per test, while increasingly facing ethical issues as well.

In vitro models are able to significantly reduce such issues by offering identical environments in numerous arrays, as well as lower cost, time and ethical constraints. Thus, the development of valid *in vitro* models can facilitate the overall drug development process by acting as a pre-cursor, or even a replacement, for animal studies.

The validity of an *in vitro* model is dependent on how well it reproduces the key physiological and biological characteristics of its *in vivo* archetype (Fig. 1B). The key characteristics of the BBB include: (1) the primary structure, consisting of strongly expressed tight junctions between endothelial cells which directly control compound permeability;[28] (2) co-culture of endothelial cells with astrocytes including endfoot contact, which plays an important role in modulating barrier function through cell-cell signaling;[29] (3) mechanotransductive effects of shear stress from fluid flow on endothelial cells, which is known to critically influence cell differentiation and tight junction formation;[30,31] (4) selective permeability from the constituted structures to dissolved compounds; (5) maintenance of high electrical resistance representing the maturity and soundness of the structures.

To mimic such key characteristics, various *in vitro* models have been developed to date[4–17] and can be mainly divided into two groups: static and dynamic models, defined by the inclusion of fluid flow, resulting in shear stress over the surface of the cells. Static models have been the most widely used since the first transwell setup in 1991.[6,14] Recently, dynamic *in vitro* BBB (DIV-BBB)[15–17] models have been developed which utilize hollow fibers to mimic the BBB architecture and flow conditions, providing

Table 1 Qualitative comparison of standard BBB models with the μBBB proposed in this article

Experimental system	*In vivo* models	*In vitro* models		
System type	Animals	Transwells	DIV-BBB	μBBB
Citations	1–3	4–13	14–17	18, this work
Relative cost	High	Very Low	Low	Low
Massively-parallel, controlled, and repeatedly identical	No	Yes	Yes	Yes
Shear stress/dynamic flow	Yes	No	Yes	Yes
(Quantitative analysis)	(No)	—	(Yes)	(Yes)
Space between co-cultures	Immediate	<10 μm	>150 μm	<10 μm
Functional media volumes	N/A	0.5–2 ml	1.4 ml	12 μl
Time to steady-state TEER	N/A	3–4 days	9–12 days	3–4 days
TEER electrodes – Ion flow profile	Invasive	Uniform {EndOhm}	Non-uniform	Uniform
(Gap size)		(<2 mm {EndOhm})	(>1 cm)	(<400 μm)
(Fixed position)		(No)	(Yes)	(Yes)
Non-destructive microscopy	No	Yes	No	Yes
Fabrication	N/A	Simple	Complex	Moderate

adequate shear stress. However, wall thickness (150μm) is significantly higher than transwell thickness (10μm), discouraging cell-cell interaction, and DIV-BBBs take significantly longer to reach steady-state TEER values[15,32] than static transwell models. To our knowledge, no existing BBB systems have addressed each of these shortcomings yet.

In order to address the issue, we have developed a microfluidic BBB (μBBB)[18] that includes each of the following advantages over existing *in vivo* and *in vitro* static and dynamic BBB Models (Table 1): (1) significantly lower costs and timescales than *in vivo* studies; (2) massively-parallel, controlled and repeated environments not available with *in vivo* models; (3) dynamic microenvironment providing shear stress stimulation to the cells, and allowing the improved analysis of test compounds and controlled delivery compared to static models; (4) much thinner culture membrane, decreasing the distance between co-cultured cells from DIV-BBB models. In addition, the developed μBBB model uses smaller functional volumes for quicker media exchange and material conservation. Shorter times to steady-state TEER levels allow a more rapid turn-around time, shortening experiments and allowing a more high-throughput approach to experimentation. The developed μBBB also enables installation of high-density electrodes with tiny (200 μm) gaps between either electrode and the cell layers, with uniform ion flow density, minimizing background resistance and error. Non-destructive microscopy of the system is possible by carefully designing electrode locations, due to transparency of the substrate. Finally, the developed μBBB is polymer-based, allowing comparatively rapid and low-cost fabrication.

This paper reports the detailed design, fabrication, and characterization of the developed *in vitro* dynamic thin-membrane μBBB system including multi-layered polymer fabrication, cell culturing procedure, validation of the developed models through optical imaging, static and transient permeability tests, and TEER measurements under different concentrations of various tracers.

Structure and fabrication

Structure

The developed μBBB is a multi-layered microfluidic device comprising four PDMS substrates, two glass layers, and a porous polycarbonate membrane sandwiched at the center between the PDMS layers (Fig. 2A). The assembled device houses two perpendicularly-crossing channels to introduce dynamic flows, a porous membrane at the intersection of the flow channels for cell culture, and multiple embedded electrodes to monitor TEER across the barrier. The channels are 200 μm high, and 2 mm (luminal) or 5 mm (abluminal) wide at the cell culture interface ensuring laminar flows. The porous membrane is located at the channel junction has an area of 10 mm^2 (Fig. 2B–C). The abluminal channel has a high aspect ratio (10 : 1) to promote uniform shear stress distribution across endothelial cells, and the luminal channel is significantly wider to minimize shear stresses on the astrocytes. Opposite the membrane on each side are two sets of two AgCl thin-film TEER electrode pairs forming a four-point sensing structure. The areas of the current electrodes are designed to be proportional (75%) to the cell culture area in order to encourage uniformly distributed ion flow. For interconnection, there are two pairs of fluidic and electrical I/Os, respectively.

Fabrication

The μBBB was fabricated by sequentially bonding the four patterned PDMS sub-layers, two embedded electrode layers, and the sandwiched polycarbonate membrane, resulting in a fully integrated device (Fig. 3). First, electrode layers were produced by cleaning 1 mm glass slides with piranha etch, and sputter depositing (Denton Discovery 18) thin-film electrodes with 20 nm Cr, 150 nm Au, and 800 nm Ag. Instachange marking film (3M) was patterned with a laser patterning system (Universal) to be used as a sputter mask. Silver surface was chlorinated chemically with $FeCl_3$ for 60 s at room temperature to generate an electrochemically active AgCl surface. Glass slides were diced (Disco DAD641) to 18 mm by 25 mm and embedded in 3 mm thick PDMS and cured at 65° for 2 h. Four I/O holes (0.5 mm) were cored in the top layers by punching.

To produce the channel feature layers, PDMS pre-polymer was spin-coated at 288 RPM for 1 min and cured at 65 °C for 2 h to produce 200 μm sheets, and features were laser-patterned. Polycarbonate sheets (400 nm pores, 10 μm thick) were cut from transwells (Corning) to 5 × 10 mm rectangles. The top and bottom PDMS layers, the polycarbonate sheets, and the PDMS channel layers were bonded using spin-coated and stamped 50 : 50 ratio PDMS pre-polymer : toluene as previously described.[33] Copper wire was bonded to bond-pads with silver epoxy for electrical connections.

Cell culture

In order to form a dual-layer BBB on the chip, co-culture of endothelial and astrocytic cells was performed by seeding on both sides of the porous membrane in the fabricated device by flowing cell suspensions. Specifically, b.End3 (endothelial) and C8D1A (astrocyte) cell lines were employed utilizing standard mammalian tissue culture methods for their ease of use.

The fabricated μBBB platform was sterilized and adhesion-seeded by steadily perfusing for up to seven days. Gas-permeable manifold tubing (0.25 mm ID) was attached to 22½ gauge needles and 10 μl pipet tips. Tips were sealed to theinlet holes with silicone sealant (DC734), and chips were connected to a 205S peristaltic cartridge pump (Watson-Marlow) for fluid manipulation (Fig. 4). 250 μl 8-well strips were used as reservoirs, covered with gas-permeable TFE/silicone plugs (BioTech Solutions). Chips were perfused with 70% ethanol to prevent contamination. To facilitate cell adhesion, the membrane was coated with 10 $\mu g\ ml^{-1}$ fibronectin for 2 h, then filled with growth medium and fully cleared of bubbles prior to cell seeding.

Next, the platforms were first seeded on the abluminal side with astrocytes at the concentration of $6e^4\ cm^{-2}$ by flooding concentrated cell suspension ($3e^6\ ml^{-1}$) in the abluminal chamber and inverting the devices at zero flow for two hours. Before seeding endothelial cells, the μBBB was perfused with medium at 1.3 $\mu l\ min^{-1}$ for two days.

Then, b.End3[34] cells were secondly seeded at the concentration of $6e^4\ cm^{-2}$ in the luminal channel and allowed to adhere for two

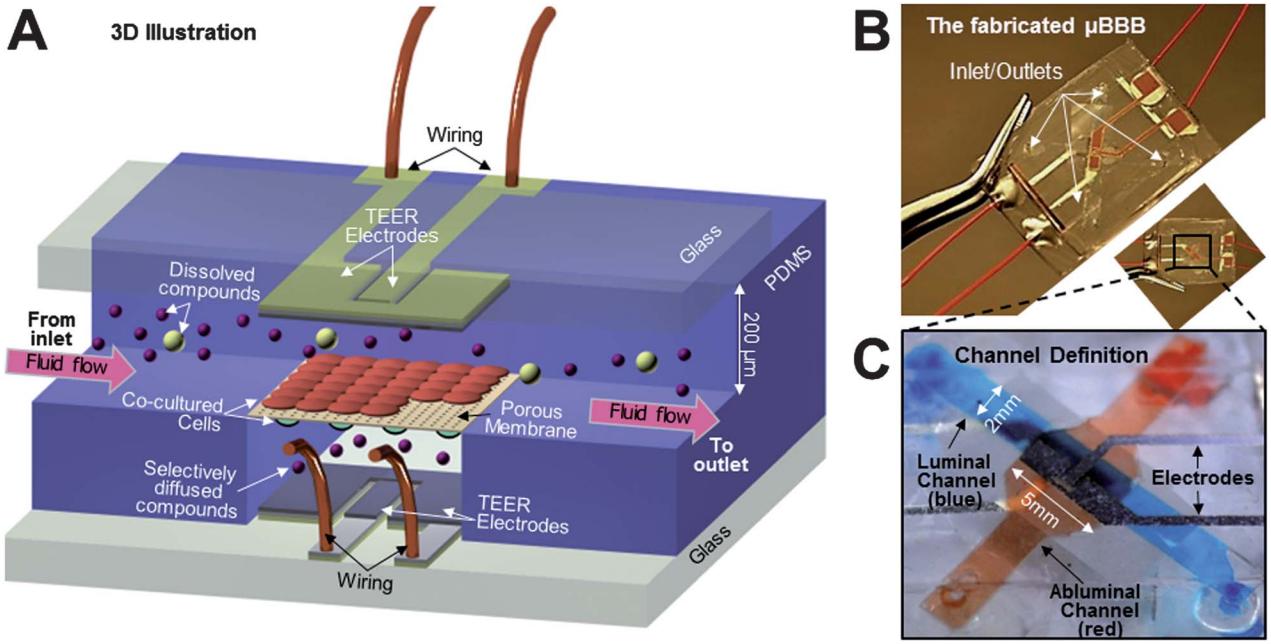

Fig. 2 Structure and design of the developed μBBB. (A) The μBBB system comprises two perpendicular flow channels. (B) The fully fabricated μBBB chip. (C) Close-up view. Channels model the lumenal (blue) and ablumenal (red) sides of the neurovascular unit. Endothelial cells and astrocytes are respectively cultured on the lumenal and ablumenal sides of the enclosed porous membrane. Channel heights are 200 μm, and channel widths are 2mm (lumen) and 5mm (albumen).

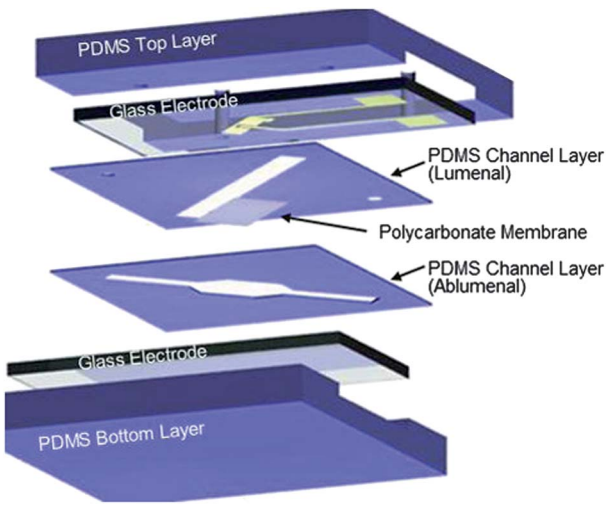

Fig. 3 Components of the μBBB. The muBBB consists of four PDMS layers, two embedded glass electrode layers, and a piece of polycarbonate membrane.

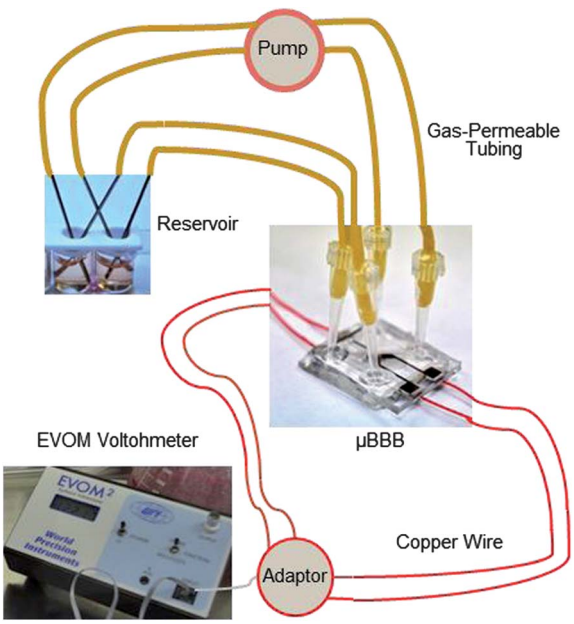

Fig. 4 Testing setup for validating the μBBB. Fully assembled μBBB includes gas-permeable tubing run through a peristaltic pump to a plugged reservoir for each channel. Electrode wiring is connected through an electrode adaptor to an EVOM Epithelial Voltohmeter for TEER measurement.

hours before rinsing with medium perfused at 1.3 μl min^{-1} for 12 h, followed by 2.6 μl min^{-1} subsequently.

Note that cells used for seeding BBB models were taken from confluent cultures (after D3 after passage) only. Static BBB models were tested by seeding astrocytes at $6e^4$ cm^{-2} on the underside of transwells (Corning) pre-treated with 10 μg ml^{-1} human fibronectin (Cultrex) in PBS for 2 h and allowed to adhere for 2 h, then cultured for 2 days prior to endothelial cell seeding on the topside at $6e^4$ cm^{-2}.

All cell cultivation and BBB experiments, including the devices and pump assembly, were carried out in a Nu-Aire Autoflow 4750 incubator which maintains a constant interior environment at 5% CO_2 and 37 °C, as indicated by internal temperature and CO_2 sensors in the incubator, with certified accuracies of +0.0125 °C and +0.1%, respectively. Cell suspensions were centrifuged in an Eppendorf 5810, and sterile work

was done in a class II biosafety cabinet (Thermo Fisher). Media used for all procedures was DMEM:F12 (CellGro), supplemented with 10% FBS (Hyclone), 1% Penicillin/Streptomycin, and 1% Fungizone (EMD). Media was buffered (NaOh or HCl buffers) to pH 7.4 (VWR sympHony) and sterile-filtered for all experiments, except for experiments in which media was buffered to pH 10. All media was supplemented with 1.2 g L^{-1} sodium bicarbonate to minimize changes in pH, though any changes in pH over the course of μBBB experiments were not measured due to volume limitations of the pH meter. The endothelial cell line b.End3 and astrocytic cell line C8-D1A were received from ATCC.

Testing methodology

To validate the fabricated μBBB system, the three most common methods were employed:[35] (1) *Cell imaging* to observe structure and morphology, (2) *TEER levels* to evaluate cell confluence and tight junction integrity, and (3) *permeability assays* to evaluate barrier selectivity. Cells were imaged with a Live/Dead assay to verify cell viability, and immunostained to look at expression of astrocyte marker GFAP and tight junction component zonal occluding-1 (ZO-1). TEER was measured as an indicator of cell confluence and tight junction integrity, with time to maximum TEER being indicative of BBB development time. Fluxes of fluorescent-labeled tracer molecules were measured to assess permeability to larger solutes. To observe the system's response to environmental changes, cells were exposed to histamine during TEER measurement and high pH during permeability assays. Real-time TEER was measured in co-cultured μBBB models during exposure to histamine (Calbiochem) at 100 μM and 150 μM concentrations. Permeability was measured in μBBB models exposed to DMEM:F12 media with elevated pH (>10) for 4 h.

Imaging

Light-phase and ESEM imaging were used for morphological observations, Live/Dead assay was used to assess viability, and immunostaining was used to look at expression of glial and tight junction marker proteins GFAP and ZO-1. To assess viability of cultured cells, Live/Dead (MGT) solution was incubated for 90 min and imaged using a Nikon fluorescence microscope. For immunostaining of both cell types, cells were fixed with 4% paraformaldehyde (Avantor) for 10 min at room temperature. Cells were permabilized with 0.1% Triton X-100 in PBS for 10 min and blocked with 5% goat serum (Rockland) and 1% unconjugated goat anti-mouse IgG $F(ab')_2$ fragment (ImmunoPure) in permeabilization buffer for 1 h. Cultures were incubated with primary antibody in blocking solution overnight at 4 °C. Cultures were rinsed with blocking solution and left in secondary antibody for 1 h, counter-stained with DAPI (Enzo) for 5 min, and imaged with a Nikon fluorescence microscope. Mouse anti-ZO-1 (Invitrogen) was used in conjunction with Alexa Fluor 488 goat anti-mouse secondary antibody (Invitrogen). Rabbit anti-GFAP (Invitrogen) was used in conjunction with Alexa Fluor 488 goat anti-rabbitt secondary antibody (Invitrogen). For imaging with environmental SEM (FEI Quanta 600 FEG), astrocyte cultures were rinsed and fixed in 4% paraformaldehyde solution for 24 h at 4 °C.

TEER measurement

Over the course of BBB experiments, TEER was measured twice a day to monitor cell confluence and development of tight junctions. For measurement of TEER, voltage and current electrode wires were connected *via* an electrode adaptor (WPI) to an EVOM2 epithelial voltohmeter (WPI). The EVOM2 passes a constant 10 μA AC current at 12.5 Hz while measuring resistance. To calculate TEER, initial D0 Background resistances R_b were subtracted from total resistance R_C at each time point and normalized for area, giving TEER values in Ω cm^2 as in the following equation.

$$TEER = (R_C - R_b)A \quad (1)$$

For real-time data collection during histamine exposure, the EVOM2 was connected to LabView on a PC *via* a data acquisition device (Texas Instruments). TEER of transwell cultures were measured daily by placing them in an Endohm chamber (WPI) and connecting it to the EVOM2.

Permeability

To assess barrier permeabilities to large compounds, fluxes of fluorescent tracers over a wide range of sizes were measured after steady-state TEER has been reached under each variant condition: monolayer, co-culture, and co-culture with elevated pH. The permeability of the system to dissolved compounds is detected by measuring the rate of diffusion across the membrane. After D3 of endothelial culture, FITC-Dextrans 4k, 20k, 70k (Sigma), and propidium iodide (Biotium) were passed at a concentration 500 μg ml^{-1} in media through the luminal channel of each device, and blank media was passed through the abluminal channel. The level of fluorescence in the media collected from the abluminal channels were measured using a BioRad Synergy Plate Reader, and converted to concentration according to prepared standards. Solute flux J_s was calculated by dividing concentration change by assay time. Permeability coefficients were calculated using the conventional equation for permeability[36]

$$P = \frac{J_s}{AC_L} \quad (2)$$

where P is the permeability coefficient, J_s is solute flux across the membrane, A is membrane area, and C_L is concentration on the luminal (source) side of the membrane. Epithelial coefficients P_e were calculated by subtracting the inverse of the overall P value by the inverse of coefficient P_b from a blank membrane, as in the following equation for permeability normalization.[37]

$$\frac{1}{P_e} = \frac{1}{P} - \frac{1}{P_b} \quad (3)$$

All permeability assays were conducted after day 3 of endothelial culture. Assays were conducted for both monolayer and co-cultured devices. To evaluate the effect of pH elevation on permeability, assay was repeated with cultures exposed to media containing pH > 10 for 4 h.

Results and discussion

The measurements indicated the validity of the developed μBBB model as an effective *in vitro* model system for studies of barrier function and drug delivery. The generally recognized characteristics of a valid *in vitro* BBB model include practicality and ease of use, *in vivo*-like cell morphology, functional expression of BBB-specific proteins, and a restricted paracellular pathway as indicated by high TEER and low permeability to compounds.[38] The b.End3 cell line has been previously characterized as having acceptably high functionality of P-glycoprotein transporter, as well as expression of numerous transporters.[34] Finally, the restrictive paracellular pathway was demonstrated by TEER levels over 250 Ωcm^2 and tracer permeabilities comparable to previous BBB models.[37]

Imaging

Imaging results were indicative of *in vivo* like morphologies for both cell types, validating structural requirements for BBB. Results from Live/Dead assays conducted on D3 of endothelial culture on μBBB membranes indicated high cell viability (>90%) of endothelial cells cultured in the system (Fig. 5A) Similar cell survival was seen for astrocytes cultured in the system. Immunostains of b.End3 cells cultured in the system revealed distinct expression of tight junction component ZO-1 by day 3 of culture (Fig. 5B). Immunostains on D2 typically lacked as clearly distinct expression of ZO-1 as seen on day 3–4, suggesting a three day minimum for full barrier development, consistent with the TEER results. Evaluation of the endothelial monolayer structure of b.End3 cells confirmed previous analysis on the cell line as valid for BBB models,[34] that tight junctions were readily expressed by day 3 of culture in the system, even without astrocyte co-culture.

Morphological analysis of the C8-D1A cell line was necessary due to a lack of described previous models using the cell line. The C8D1A cell line regularly expressed an astrocytic morphology with distinct neurites. Immunostains of C8D1A cells revealed expression of GFAP, which is a marker specific to astrocytes (Fig. 5C). ESEM of astrocytes cultured on polycarbonate membrane revealed good adhesion to the substrate (Fig. 5D), though the neurites were typically wider (>1 μm) than the pore diameter (0.4 μm), so it is unlikely that endfeet were able to mi grate through the pores. Further study should be performed to find a feasible membrane with large enough pores to encourage direct cell–cell contact between cell types, while not large enough to introduce problems with adhesion or cell migration through the membrane.

Note that the experimental setup was small enough for the entire pump system to be placed in the incubator and kept at 37 °C, and up to 4 devices could be run simultaneously with our 8-channel pumphead. Imaging indicated that both cell types exhibited characteristics desirable for BBB study, and cells are co-cultured in close contact.

TEER

TEER results indicated acceptably high[39] electrical resistance for BBB models, with conveniently short time to steady-state TEER levels, and effectively demonstrated a transient response to histamine. For both static transwell experiments and dynamic

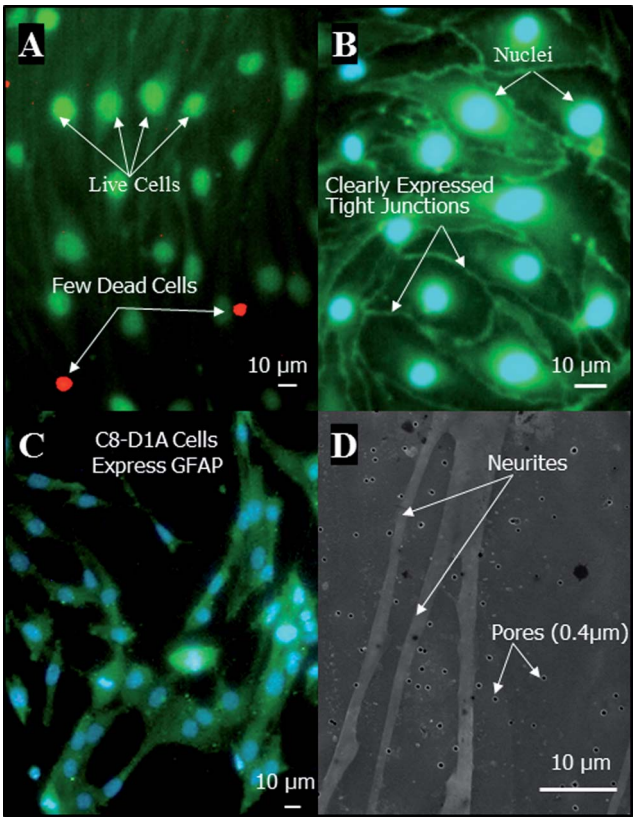

Fig. 5 Representative images of cells in μBBB. (A) Live/Dead stain (green:live, red:dead) of bEnd.3 cells on day 3 of culture on μBBB membrane indicates high cell viability. (B) Immunostains of tight junction component ZO-1 (green) in bEnd.3 cells on day 3 indicate distinct tight junction expression. Nuclei counter-stained with DAPI (blue). (C) Immunostains of GFAP (green) in C8-D1A cells reveal astrocytic morphology on polycarbonate membrane. Nuclei counter-stained with DAPI (blue). (D) ESEM of C8-D1A neurites on porous polycarbonate membrane.

μBBB cultures, cultures typically reached steady-state levels by day 3–4 of endothelial cell culture (Fig. 6). This is indicative of full tight junction development, in congruence with the ZO-1 imaging data, so day 3 was the minimum threshold for endpoint testing such as permeability assays, immunostains, and TEER response assays. For both systems, co-culturing endothelial cells with astrocytes significantly increased the steady-state TEER levels, as indicated by the arithmetic means over several runs shown in Fig. 6.

Steady-state TEER measurements. The steady-state TEER values in dynamic μBBB chips were significantly higher than our static transwell controls (Fig. 7) using the same cell lines, media formulations, and voltohmeter. TEER levels of μBBB co-cultures regularly exceeded 250 Ω cm^2, compared to only 25 Ω cm^2 in transwell co-cultures. Supported by previous studies reporting shear stress effects on endothelial cells,[31,40–49] we reasonably hypothesize that this significant increase in TEER may be due to the effects of shear stress on endothelial cells. Shear stress has a known mechano-transductive effect on endothelial molecular pathways,[44,45,48] and has been seen to up-regulate expression of tight junction proteins[47] and increase RNA

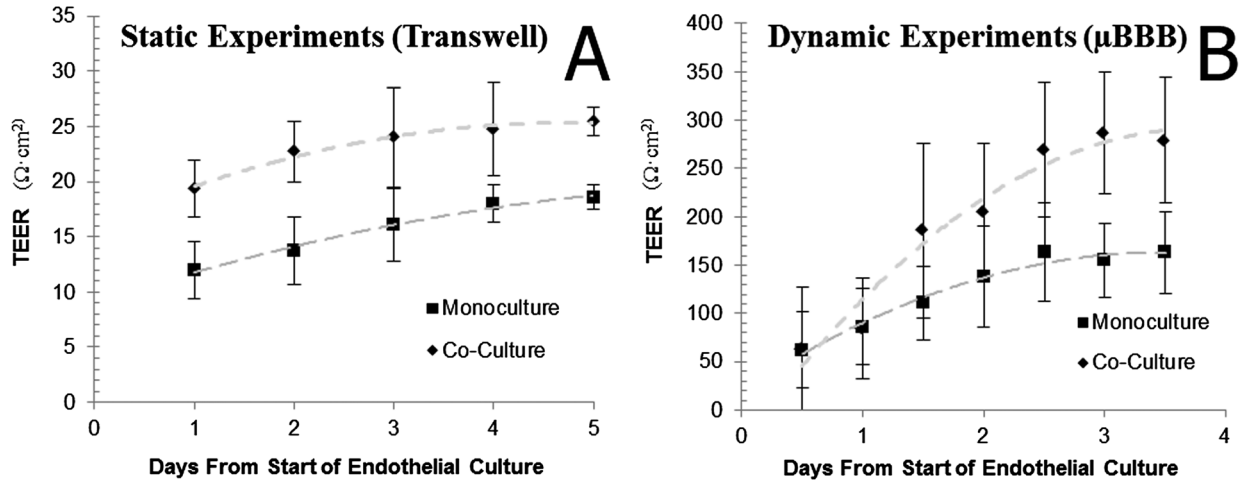

Fig. 6 TEER levels of static and dynamic experiments over time, beginning on D0 of endothelial culture. (A) TEER development of transwells seeded with b.End3 cells in monoculture and in co-culture with astrocytes. (B) TEER development of μBBB devices seeded with b.End3 cells in monoculture and in co-culture with astrocytes. Both systems typically reached steady-state TEER by D3 of culture. All $n > 3$.

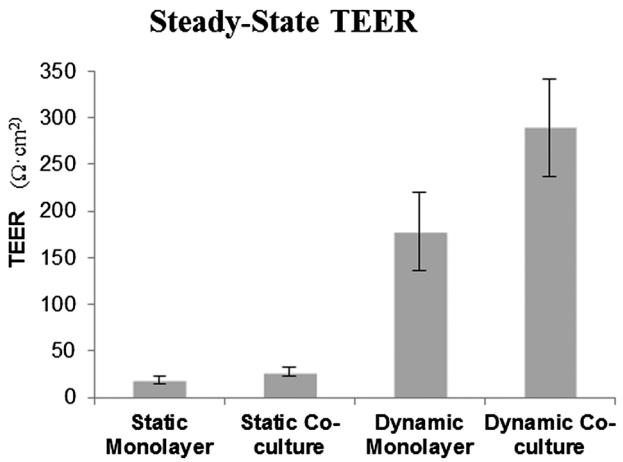

Fig. 7 Steady-state TEER levels of each base condition. Dynamic cultures reached significantly higher TEER levels than static cultures. For both systems, co-cultures developed higher TEER levels than endothelial monolayers alone.

levels of BBB transporter proteins[30] in vascular endothelial cells, modulate cytoskeletal structure,[31,42] and shows less inflammatory effects with definitive directional flow[46] than disturbed flow.[49]

However, other differences exist between the μBBB system and our transwell controls which may factor into differences in results, such as total cell numbers and media volumes, culture surface/volume ratios, ratio between endothelial cells and astroctyes, and TEER electrode characteristics such as size, gap, and orientation.

Though *in vivo* TEER levels are greater than 1000 Ω cm^2, a consensus has been reached that for a system showing sufficiently high TEER levels over 150 Ω cm^2, reasonably representative data can be obtained,[39] while our system typically exceeded 250 Ω cm^2.

Dynamic TEER measurements. A transient drop and recovery to the original levels in TEER was observed as a result of exposure to histamine (Fig. 8), indicating the robustness of the model for repeated at long-term testing purposes. The drop occurred very rapidly upon exposure to histamine, and TEER returned to initial levels within six minutes at 100μM histamine concentration, and fifteen minutes for 150 μM concentrations. Maximum TEER drop was approximately 30% for 100 μM histamine, and 50% for 150 μM histamine. A similar transient response of endothelial cells to histamine has been reported in previous studies.[50–54] This effect has been attributed to brief formation of *trans*-endothelial gap formation,[55] and has also been suggested to be due to increased *trans*-cytosis.[56] The ability to observe real-time transient changes in TEER without disturbing the system is a significant practical advantage of our system.

Permeability

Permeabilities of μBBB cultures to large molecules were shown to be selective according to size, and seen to be slightly lower for co-cultures than endothelial cells alone, and found to be higher when pH is significantly elevated. The μBBB system is advantageous for permeability assays, because eqn (2) assumes tracer concentrations are kept constant, which is not necessarily true for static models in which concentrations in both chambers change with time. This is a valid assumption for flow-based BBB models, because fresh media at constant concentration is continuously delivered to the chamber. Permeability coefficients of Dextrans 4 kD, 20 kD, and 70 kD, and propidium iodide were calculated and plotted according to stokes radius, or the radius of a sphere with the same diffusive properties (Fig. 9). Results for all conditions showed higher permeability to tracers of lower stokes radius, indicating that smaller compounds pass through junctions easier. Co-cultured systems showed lower permeability than for monoculture of endothelial cells alone, consistent with the higher TEER levels. Exposing μBBB co-cultures to significantly higher pH levels (>10) for 4 h led to significantly higher permeabilities to all tracers, indicating loss of barrier function. This increase in permeability due to heightened pH has been

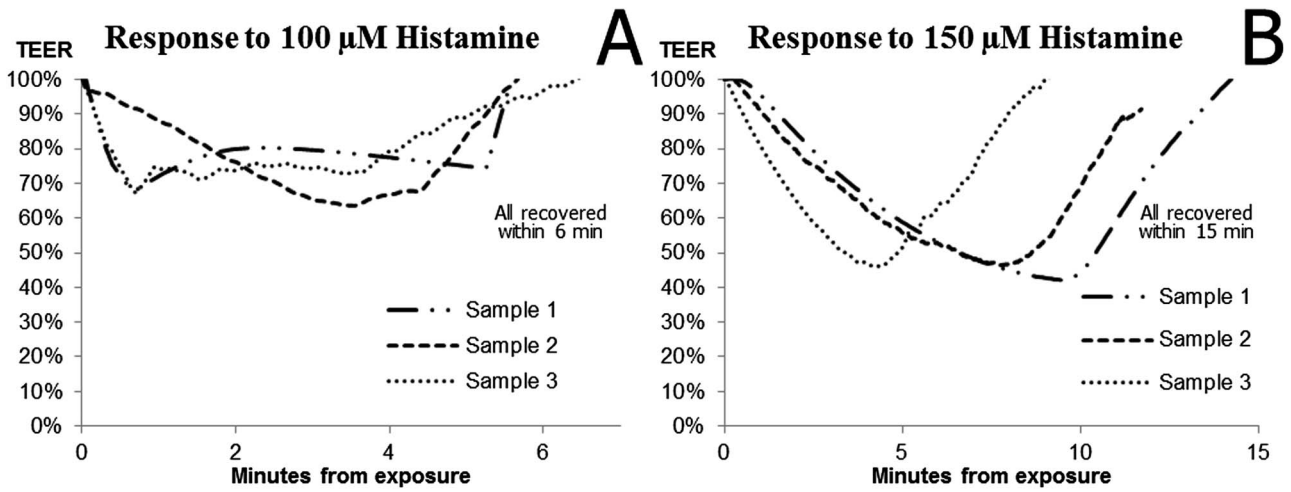

Fig. 8 Continuous response to histamine exposure in three samples at each concentration. Co-cultured µBBB on D4 were perfused with histamine at two concentrations. (A) Three samples perfused with 100 µM histamine saw a transient drop of up to 30% over a period of 5–7 min. (B) Three samples perfused with 150 µM histamine saw a transient drop of up to 50% over a period of 8–15 min.

observed in previous BBB models,[57,58] and is indicative of a drop in barrier function. However, permeabilities for both co-cultures and endothelial monoculture were higher than those previously reported from *in vivo* studies.[2] To our knowledge, results from a BBB model with permeability levels as low as *in vivo* have yet to be achieved.

Conclusions

We have developed a µBBB that effectively mimics the dynamic cerebrovascular environment with fluid shear stress, and the results from this characterization study indicate that the model expresses sufficient key characteristics of a BBB model. Tight junction expression in the b.End3 cells and GFAP expression were characteristic of *in vivo*. The µBBB showed significantly higher TEER levels than in static models, with a comparatively short time to steady state TEER to the DIV-BBB system. Real-time TEER response was shown to be feasible through measurement of transient effects histamine testing. Permeability assays were demonstrated in the system, with a selective permeability over a wide range of tracer sizes. These characteristics indicate that the µBBB system is a useful and enabling tool for

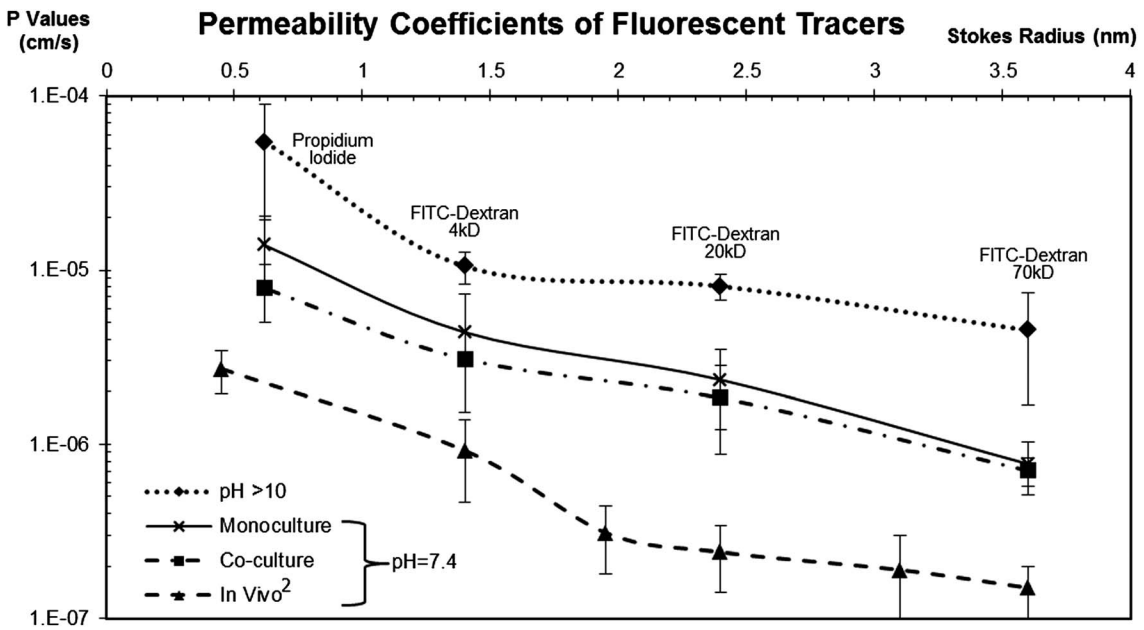

Fig. 9 Permeabilities of cultured µBBB under different conditions. Tracer molecules FITC-Dextrans 4k, 20k, 70k, and propidium idodide reveal selectivity according to size. Also plotted for reference is *in vivo* data from a previous study[2], which showed a lower permeability curve than all *in vitro* models. Co-cultures showed lower permeability than monocultured b.End3 cells alone. Increasing pH to 10 for 4 h resulted in significantly increased permeabilities. All $n > 3$.

further studies of BBB function and delivery. It can be used to monitor changes in barrier function in response to various environmental stimuli, such as barrier-enhancing or barrier-opening drugs. Finally, through permeability assays the system can be used to predict the rate of delivery of new drugs across the BBB. Thus, we believe use of the fabricated μBBB is a valid option for pre-clinical studies.

Acknowledgements

This research was supported by the Utah Science Technology and Research Initiative (USTAR) and the DARPA Young Faculty Award 2011 (N66001-11-14149). Microfabrication was performed at the state-of-the-art University of Utah Nano Fabrication Facility located in the Sorenson Molecular Biotechnology Building.

References

1 S. Soni, A. K. Babbar, R. K. Sharma and A. Maitra, *J. Drug Targeting*, 2006, **14**, 87–95.
2 W. Yuan, Y. Lv, M. Zeng and B. M. Fu, *Microvasc. Res.*, 2009, **77**, 166–73.
3 E. Preston, J. Slinn, I. Vinokourov and D. Stanimirovic, *J. Neurosci. Methods*, 2008, **168**, 443–9.
4 C. Weidenfeller, C. N. Svendsen and E. V. Shusta, *J. Neurochem.*, 2007, **101**, 555–65.
5 S. Nakagawa, M. A. Deli, H. Kawaguchi, T. Shimizudani, T. Shimono, A. Kittel, K. Tanaka and M. Niwa, *Neurochem. Int.*, 2009, **54**, 253–63.
6 L. L. Rubin, D. E. Hall, S. Porter, K. Barbu, C. Cannon, H. C. Horner, M. Janatpour, C. W. Liaw, K. Manning and J. Moralesand, *et al.*, *J. Cell Biol.*, 1991, **115**, 1725–35.
7 J. Wegener, A. Hakvoort and H. J. Galla, *Brain Res.*, 2000, **853**, 115–24.
8 T. J. Raub, *Am J Physiol*, 1996, **271**, C495–503.
9 K. E. Bruckener, A. el Baya, H. J. Galla and M. A. Schmidt, *J. Cell Sci.*, 2003, **116**, 1837–46.
10 W. Neuhaus, V. E. Plattner, M. Wirth, B. Germann, B. Lachmann, F. Gabor and C. R. Noe, *J. Pharm. Sci.*, 2008, **97**, 5158–75.
11 G. Schiera, S. Sala, A. Gallo, M. P. Raffa, G. L. Pitarresi, G. Savettieri and I. Di Liegro, *J. Cell. Mol. Med.*, 2005, **9**, 373–9.
12 K. Cohen-Kashi Malina, I. Cooper and V. I. Teichberg, *Brain Res.*, 2009, **1284**, 12–21.
13 G. Li, M. J. Simon, L. M. Cancel, Z. D. Shi, X. Ji, J. M. Tarbell, B. Morrison, 3rd and B. M. Fu, *Ann Biomed Eng*, 2010.
14 L. Cucullo, P. O. Couraud, B. Weksler, I. A. Romero, M. Hossain, E. Rapp and D. Janigro, *J. Cereb. Blood Flow Metab.*, 2008, **28**, 312–28.
15 S. Santaguida, D. Janigro, M. Hossain, E. Oby, E. Rapp and L. Cucullo, *Brain Res.*, 2006, **1109**, 1–13.
16 L. Cucullo, M. S. McAllister, K. Kight, L. Krizanac-Bengez, M. Marroni, M. R. Mayberg, K. A. Stanness and D. Janigro, *Brain Res.*, 2002, **951**, 243–54.
17 W. Neuhaus, R. Lauer, S. Oelzant, U. P. Fringeli, G. F. Ecker and C. R. Noe, *J. Biotechnol.*, 2006, **125**, 127–41.
18 R. Booth and H. Kim, *International Conference on Miniaturized Systems for Chemistry and Life Sciences*, 2011, **15**, 1388–1390.
19 M. N. Pangalos, L. E. Schechter and O. Hurko, *Nat. Rev. Drug Discovery*, 2007, **6**, 521–32.
20 C. P. Ferri, M. Prince, C. Brayne, H. Brodaty, L. Fratiglioni, M. Ganguli, K. Hall, K. Hasegawa, H. Hendrie and Y. Huang, *Lancet*, 2006, **366**, 2112–2117.
21 W. M. Pardridge, W. H. Oldendorf, P. Cancilla and H. J. Frank, *Ann Intern Med*, 1986, **105**, 82–95.
22 F. L. Cardoso, D. Brites and M. A. Brito, *Brain Res. Rev.*, 2010, **64**, 328–63.
23 W. M. Pardridge, *Mol. Interventions*, 2003, **3**, 90–105, 51.
24 A. Reichel, *Chem. Biodiversity*, 2009, **6**, 2030–49.
25 L. Cucullo, B. Aumayr, E. D. Rapp and Janigro, *Curr Opin Drug Discov Devel*, 2005, **8**, 89–99.
26 B. T. Hawkins and T. P. Davis, *Pharmacol. Rev.*, 2005, **57**, 173–85.
27 S. A. Pathan, Z. Iqbal, S. M. Zaidi, S. Talegaonkar, D. Vohra, G. K. Jain, A. Azeem, N. Jain, J. R. Lalani, R. K. Khar and F. J. Ahmad, *Recent Pat. Drug Delivery Formulation*, 2009, **3**, 71–89.
28 H. Wolburg and A. Lippoldt, *Vasc. Pharmacol.*, 2002, **38**, 323–37.
29 R. F. Haseloff, I. E. Blasig, H. C. Bauer and H. Bauer, *Cell. Mol. Neurobiol.*, 2005, **25**, 25–39.
30 L. Cucullo, M. Hossain, V. Puvenna, N. Marchi and D. Janigro, *BMC Neurosci.*, 2011, **12**, 40.
31 C. G. Galbraith, R. Skalak and S. Chien, *Cell Motil. Cytoskeleton*, 1998, **40**, 317–30.
32 J. P. Frampton, M. L. Shuler, W. Shain and M. R. Hynd, *Cent Nerv Syst Agents Med Chem*, 2008, **8**, 203–219.
33 B. H. Chueh, D. Huh, C. R. Kyrtsos, T. Houssin, N. Futai and S. Takayama, *Anal. Chem.*, 2007, **79**, 3504–8.
34 Y. Omidi, L. Campbell, J. Barar, D. Connell, S. Akhtar and M. Gumbleton, *Brain Res.*, 2003, **990**, 95–112.
35 M. A. Deli, C. S. Abraham, Y. Kataoka and M. Niwa, *Cell. Mol. Neurobiol.*, 2005, **25**, 59–127.
36 W. M. Pardridge, D. Triguero, J. Yang and P. A. Cancilla, *J Pharmacol Exp Ther*, 1990, **253**, 884–91.
37 G. Li, M. J. Simon, L. M. Cancel, Z. D. Shi, X. Ji, J. M. Tarbell, B. Morrison, 3rd and B. M. Fu, *Ann. Biomed. Eng.*, 2010, **38**, 2499–511.
38 J. A. Nicolazzo, S. A. Charman and W. N. Charman, *J. Pharm. Pharmacol.*, 2006, **58**, 281–93.
39 M. Vastag and G. M. Keseru, *Curr Opin Drug Discov Devel*, 2009, **12**, 115–24.
40 O. Thoumine, R. M. Nerem and P. R. Girard, *In Vitro Cell. Dev. Biol.: Anim.*, 1995, **31**, 45–54.
41 R. M. Nerem, R. W. Alexander, D. C. Chappell, R. M. Medford, S. E. Varner and W. R. Taylor, *Am. J. Med. Sci.*, 1998, **316**, 169–75.
42 K. Ookawa, M. Sato and N. Ohshima, *Front Med Biol Eng*, 1993, **5**, 121–5.
43 S. Y. Desai, M. Marroni, L. Cucullo, L. Krizanac-Bengez, M. R. Mayberg, M. T. Hossain, G. G. Grant and D. Janigro, *Endothelium*, 2002, **9**, 89–102.
44 E. Tzima, M. Irani-Tehrani, W. B. Kiosses, E. Dejana, D. A. Schultz, B. Engelhardt, G. Cao, H. DeLisser and M. A. Schwartz, *Nature*, 2005, **437**, 426–31.
45 Y. S. Li, J. H. Haga and S. Chien, *J. Biomech.*, 2005, **38**, 1949–71.
46 S. Chien, *Biorheology*, 2006, **43**, 95–116.
47 V. Siddharthan, Y. V. Kim, S. Liu and K. S. Kim, *Brain Res.*, 2007, **1147**, 39–50.
48 S. Chien, *Am. J. Physiol.: Heart Circ. Physiol.*, 2007, **292**, H1209–24.
49 S. Chien, *Ann. Biomed. Eng.*, 2008, **36**, 554–62.
50 G. P. van Nieuw Amerongen, R. Draijer, M. A. Vermeer and V. W. van Hinsbergh, *Circ Res*, 1998, **83**, 1115–23.
51 L. Schilling and M. Wahl, *Brain Res.*, 1994, **653**, 289–96.
52 A. Gulati, K. N. Dhawan, R. Shukla, R. C. Srimal and B. N. Dhawan, *Pharmacol. Res. Commun.*, 1985, **17**, 395–404.
53 T. Takeda, Y. Yamashita, S. Shimazaki and Y. Mitsui, *J Cell Sci*, 1992, **101**(Pt 4), 745–50.
54 N. J. Abbott, *Cell. Mol. Neurobiol.*, 2000, **20**, 131–47.
55 N. Z. Wu and A. L. Baldwin, *Am J Physiol*, 1992, **262**, H1238–47.
56 M. A. Deli, M. P. Dehouck, R. Cecchelli, C. S. Abraham and F. Joo, *Inflammation Res.*, 1995, **44**(S1), S56–7.
57 H. M. Nielsen and M. R. Rassing, *Eur. J. Pharm. Sci.*, 2002, **16**, 151–7.
58 H. M. Nielsen and M. R. Rassing, *Int. J. Pharm.*, 1999, **185**, 215–25.

